J. Fluid Mech. (1999), *vol.* 389, *pp.* 1–26. Printed in the United Kingdom

Horizontal oscillations of a cylinder beneath a free surface: vortex formation and loading

By J.-C. LIN AND D. ROCKWELL

Department of Mechanical Engineering and Mechanics, 354 Packard Laboratory,
19 Memorial Drive West, Lehigh University, Bethlehem, PA 18015, USA
e-mail: dor0@lehigh.edu

(Received 15 January 1998 and in revised form 4 January 1999)

The patterns of vortex formation from a cylinder oscillating in a horizontal plane, located at various depths of submergence beneath a free surface, are characterized using high-image-density particle image velocimetry (PIV). Instantaneous representations of the velocity field, streamline topology and vorticity patterns are referenced to the instantaneous velocity of the cylinder. In turn, these features are related to the magnitude and phase of the instantaneous transverse force, which can exhibit highly nonlinear, spike-like fluctuations. When a finite gap is maintained between the free surface and the cylinder, the patterns of vorticity concentrations are altered in such a fashion that both the peak magnitude and the degree of amplitude modulation of the negative transverse force spikes are attenuated, but shifted little in phase, relative to the case of the fully submerged cylinder. On the other hand, when the cylinder is sufficiently close to the free surface such that the gap region is eliminated, the patterns of vorticity concentrations are fundamentally different and the negative transverse force spikes are remarkably more pronounced and consistent than for deeper submergence.

1. Introduction

Oscillating flow past a stationary cylinder or, conversely, a cylinder oscillating in quiescent fluid, is an effective means of simulating long wave–cylinder interaction. The Keulegan–Carpenter number $KC = 2\pi A/D$, where A is the amplitude of the motion and D is the cylinder diameter, is typically employed to describe the onset and possible modes of vortex formation. The corresponding frequency parameter is $\beta = fD^2/\nu$, in which f is the oscillation frequency and ν is kinematic viscosity.

An assessment of early investigations is given by Sarpkaya & Isaacson (1981) for a wide range of KC. A number of interesting unstable and transitional phenomena occur as KC and β are increased. These features are described by Honji (1981), Sarpkaya (1986), and Tatsuno & Bearman (1990). Possible types of vortex patterns in relation to defined values or ranges of KC are described by Singh (1979), Bearman *et al.* (1981), Sarpkaya & Isaacson (1981), Ikeda & Yamamoto (1981), Iwagaki, Asano & Nagai (1983), Williamson (1985), and Obasaju, Bearman & Graham (1988). When $KC > 4$, a degree of asymmetry in the process of vortex formation leads to both a transverse and an in-line force component. In fact, for values of KC larger than this value, a wide variety of vortex patterns can be generated, and even at a given value of KC, more than one type of pattern may be admissible. These patterns of vortices are no doubt linked to the measured (transverse) vibrations of the corresponding elastically mounted cylinder, as addressed by Sumer & Fredsøe (1986).

Numerical modelling of unidirectionally oscillating cylinders in quiescent fluid or, conversely, a stationary cylinder in oscillating flow, has been approached using a variety of methods. Baba & Miyata (1987), Wang & Dalton (1991), Justesen (1991), and Miyata & Lee (1990) employed finite-difference solutions of the Navier–Stokes equations, Anagnostopoulos, Iliadis & Ganoulis (1995) used a finite-element approach to the NS equations, and Sun & Dalton (1996) assess applied the method of large eddy simulation (LES) for solution of the NS equations. Sarpkaya (1989) and Lin, Bearman & Graham (1996) assess their own and previous approaches using discrete vortex approaches, making use of Lagrangian or mixed Lagrangian–Eulerian schemes.

Early insight into this class of vortex–body interactions is provided by Sarpkaya (1963, 1968, 1969), who derived the equations for the instantaneous transverse force and drag on a circular cylinder in a time-dependent flow, accounting for an arbitrary number of discrete vortices. Using a similar analysis, and tracking dye-visualized vortices in the immediate vicinity of the cylinder, Maull & Milliner (1978) provide substantial insight into the relationship between the formation and movement of the vortices and the variation of the measured transverse and in-line forces. This sort of approach was also employed by Ikeda & Yamamoto (1981), who approximated the strength and motion of identifiable vortices from streak-marker visualization, in order to make rough predictions of the variation of the transverse force with time. More recently, Lin & Rockwell (1996) employed quantitative images for a selected portion of the oscillation cycle. By treating the instantaneous concentrations of vorticity as point vortices, they approximated the transverse force via the Maull–Milliner (1978) approach. In addition, they calculated the transverse force using the actual distributed concentrations of vorticity by means of a vorticity moment approach described by Lighthill (1986); this technique was recently extended by Noca, Shiels & Jeon (1997) to account for situations where vorticity concentrations are convected away from the field of view. An alternative approach for determining the consequence of the vortical motion on the transverse force involves a momentum-based concept that avoids evaluation of vorticity; it involves a control volume surrounding the cylinder, as discussed by Unal, Lin & Rockwell (1997) and Noca (1997).

Relatively little is known of the flow patterns about, and loading on, a unidirectionally oscillating cylinder in the presence of a free surface, with emphasis on sufficiently high values of KC, such that pronounced vortex formation occurs, not only from the cylinder, but possibly the free surface as well. The most closely related studies are those of: Miyata, Shikazono & Kanai (1990), involving qualitative visualization and numerical simulation of steady translation of the cylinder beneath a free surface; Sheridan, Lin & Rockwell (1997) for free-surface flow past a stationary cylinder; Lin, Sheridan & Rockwell (1996) for vertical perturbations of a semi-submerged cylinder in the presence of mean flow; Miyata & Lee (1990), involving qualitative visualization and numerical simulation of vortex motions induced by wave motion past a horizontal cylinder; and Jarno-Dreuaux, Sakout & Lambert (1995) focusing on laser-Doppler velocity measurements of the vortex pattern induced by wave motion past a circular cylinder adjacent to a wall. Measurements of forces on a cylinder in proximity to a wall are provided by Tsahalis (1984, 1985), Jacobsen *et al.* (1984), and Sumer, Fredsøe & Jacobsen (1986).

In general, the quantitative structure of vortices from an oscillating cylinder in quiescent fluid has remained unclarified for varying degrees of proximity to a free surface. The degree of concentration of vorticity and the possible distortions of patterns of vorticity concentrations as the cylinder moves through regions of previously generated vorticity is essential for a complete understanding of the vortex formation

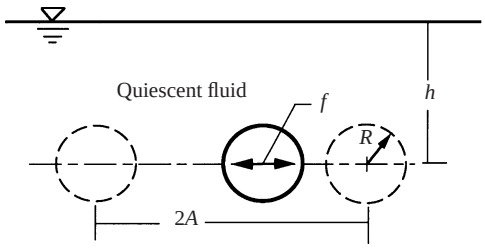

FIGURE 1. Diagram of an oscillating cylinder beneath the free surface.

process. Such knowledge of the instantaneous vorticity field, in conjunction with the instantaneous topology of the streamline patterns, can provide a quantitative basis for describing the stages of growth of a vorticity layer adjacent to an oscillating cylinder and its eventual detachment, or shedding, from the cylinder. The present study aims to define these instantaneous, quantitative features of the vortex formation process and link them to the instantaneous transverse force.

2. Experimental system and techniques

Experiments were undertaken in a free-surface water channel having a test-section 5500 mm long, 597 mm deep, and 597 mm wide, with the water level maintained at a depth of 521 mm. For the present experiments, the water was maintained in a quiescent state. A test-section insert housed the oscillating cylinder system, represented in figure 1. It had an internal length of 787 mm and a width of 495 mm. A 50.8 mm diameter cylinder having a length of 483 mm was mounted at the mid-depth location. Circular end plates were located at either end of the cylinder and immediately adjacent to the interior of the wall of the test-section insert. These end plates had a diameter of 483 mm and a thickness of 3.2 mm; they were bevelled at an angle of 30° at their edges, in order to preclude localized flow separation. This cylinder–end plate system was driven in the horizontal direction by an arm external to the test-section insert. A computer-controlled, high-resolution motor allowed arbitrary frequency and amplitude of the sinusoidal motion of the system.

The entire cylinder–endplate system was deployed at three values of submergence beneath the free surface: $h/R = 1.2$, 1.9, and 10. The value of $h/R = 10$, corresponding to the plane of symmetry of the test-section, is taken to represent the fully submerged state. The general form of the patterns of vortices is in accord with those of Williamson (1985) and Obasaju *et al.* (1988), who employed different experimental arrangements. Moreover, comparison of the time histories of the in-line and transverse force fluctuations of the latter investigation with those of the present study indicate remarkable similarity of both form and amplitude. Values of $h/R = 1.2$ and 1.9 were selected after extensive preliminary visualization. It indicated that, at these depths of submergence, distinctly different modes of vortex formation could be observed, relative to the classical mode at $h/R = 10$. The distinctive mode at $h/R = 1.9$ is representative of that occurring for the case of a small gap between the cylinder and the free surface. The mode at $h/R = 1.2$ represents zero gap, owing to a local depression of the free surface above the cylinder during oscillation; it therefore corresponds to zero flow between the cylinder and the free surface.

All experiments were performed at a value of Keulegan–Carpenter number $KC = 2\pi A/D = 10$. The frequency of the cylinder motion was $f = 0.14$ Hz, giving a dimen-

sionless value of the frequency parameter $\beta = fD^2/\nu = 378$. The effective Reynolds number was $Re = KC\beta = 3780$. The value of $KC = 10$ generates generally repeatable patterns of asymmetrical vortices (Sarpkaya & Isaacson 1981; Williamson 1985; Obasaju *et al.* 1988), and thereby significant values of transverse force. Moreover, Obasaju *et al.* (1988) show that the spanwise correlation of the fluctuating surface pressure is very high at $KC = 10$, indicating nearly two-dimensional vortex formation. Extensive, preliminary experiments using hydrogen bubble and dye visualization at all depths of submergence of the cylinder showed quasi-two-dimensional vortex formation, with the exception of small-scale streamwise vorticity. In addition to the foregoing parameters KC, β and Re, typically employed for a fully submerged cylinder undergoing oscillatory motion, the Froude number $Fr_1 = U/(gD)^{1/2}$ or $Fr_2 = U/(gh)^{1/2}$ must be specified; U is the maximum velocity of the cylinder, and D and h are the cylinder diameter and the gap between the cylinder and the free surface, respectively. For the present experiments, $Fr_1 = 0.103$ and $Fr_2 = 0.046$, 0.105, and 0.133, corresponding to the respective values of $h/R = 10$, 1.9, and 1.2. For all of these values of Fr, the free surface was essentially undisturbed, except for a small-scale surface depression above the cylinder at the smallest value of $h/R = 1.2$.

The instantaneous transverse force L was measured using a pressure integration technique described by Szepessy & Bearman (1993); this led to the transverse force coefficient (per unit length) $C_L = L/(\frac{1}{2}\rho U_0^2 D)$. A total of eight pressure taps were located about each half circumference of the cylinder. Each set of taps was connected to a common reservoir, such that the average pressure over half the cylinder was obtained with insignificant distortion and phase shift. Then, by subtracting the integrated pressure obtained on opposing sides of the cylinder, the net instantaneous transverse force was obtained. A detailed set of design guidelines, including pressure tap spacing, as well as a critical assessment of this technique, is provided by Szepessy & Bearman (1993). The pressures on each half of the cylinder were sensed by two PCB 106B50 high-sensitivity pressure transducers, custom designed for immersion in water. The outputs of these transducers were amplified, then filtered, at the inputs of the A/D interface board of the laboratory microcomputer. Detailed tests with reference signals and associated calculations showed that the amplitude and phase distortion, induced by the sequential instrumentation from the output of the pressure transducer to the memory of the microcomputer, was less than 0.5% of the original signal.

Determination of the instantaneous velocity fields, streamline patterns and distributions of vorticity was accomplished using a laser-scanning version of high-image-density particle image velocimetry, described by Rockwell *et al.* (1993). A 20 W, continuous-wave argon-ion laser was directed against a rotating mirror with 72 facets, thereby generating a scanning laser beam, which formed a well-defined sheet. This approach generated a laser scanning frequency of 361 $\mathrm{c\,s^{-1}}$. The scanning beam was located a distance of $3.5D$ from the midplane of the cylinder. The plane of the pressure taps was located a distance of $\frac{7}{16}D$ from the laser plane, thereby providing sectional values of transverse force, which were nearly coincident with the sectional development of the vortex formation from the cylinder. This approach precludes difficulties associated with force transducer measurements that include cylinder end effects.

The water was seeded with 12 μm diameter hollow glass spheres, which were coated with a thin layer of silver. Particle images were recorded using a Nikon F-4 camera with a 105 mm lens. High-resolution 35 mm film (300 lines $\mathrm{mm^{-1}}$) was employed as a recording medium. The entire system, comprising the camera, bias mirror and motion of the cylinder, was controlled by the same laboratory and microcomputer that acquired the instantaneous pressure data.

The lens system, corresponding to a magnification $M = 1:8.3$, represents the ratio of the lengthscale on the film negative to the lengthscale in the physical plane of the laser sheet. The 35 mm negatives of the patterns of particle images were digitized using a film scanner having a resolution of 125 pixels mm^{-1}. With these digitized images at hand, it is possible to obtain the velocity vectors. This was accomplished using interrogation of a window size of 90 pixels $\times$ 90 pixels (0.72 mm $\times$ 0.72 mm)with 50% overlap. In order to satisfy the criterion of high image density, each interrogation window contained approximately 80 to 100 particle images. Evaluation of this pattern of images yielded one velocity vector by use of a single-frame, cross-correlation approach. The foregoing parameters corresponded to an effective grid size of 0.36 mm $\times$ 0.36 mm on the film and, with the given value of magnification M, a grid of 3 mm $\times$ 3 mm in the plane of the laser sheet. A critical assessment of the effect of grid size m the patterns of velocity and vorticity of this class of flow is given by Lin & Rockwell (1997). Larger grids than employed herein obscure the important features of the small-scale patterns of vorticity in the immediate vicinity of the cylinder.

Simultaneous acquisition of PIV images and the transverse force involved synchronization of the force acquisition with the trigger for the camera shutter. Data acquisition commenced at completion of the fiftieth cycle of the cylinder oscillation. This number of cycles allowed adequate development of the flow unsteadiness. In all force traces exhibited herein, $t = 0$ corresponds to the extreme position of the cylinder. At this instant, the camera was triggered and, after a mechanical delay, sent out a signal to start acquisition of the force data (see figures 2 and 3).

3. Force signatures

The instantaneous transverse force coefficient $C_L = L/(\frac{1}{2}\rho U_0^2 D)$ is shown in figure 2 as a function of dimensionless time t/T, in which T is the period of the cylinder oscillation. Three traces are given for different dimensionless depth h/R of submergence beneath the free surface, in which h is measured from the free surface to the centre of the cylinder and R is the cylinder radius. At $h/R = 10$, the cylinder is essentially fully submerged beneath the free surface. Two cycles of modulated transverse force occur for each cycle of the cylinder motion. This modulated pattern, the relative magnitudes of the negative peaks of C_L, and their phase relative to the instantaneous velocity U of the cylinder, are in general agreement with C_L by the traces of Obasaju *et al.* (1988), for which the mode-averaged total force along the span was measured, in contrast to the instantaneous, sectional force measurement of the present study. This observation reaffirms the quasi-two-dimensional nature of the loading and thereby the flow physics at $KC = 10$, already suggested by their high spanwise correlations of fluctuating pressure noted in the foregoing. For decreased submergence, represented by $h/R = 1.9$, both the degree of modulation and the magnitude of the negative peaks of C_L are decreased, relative to the aforementioned case. When the cylinder is located very close to the free surface, however, represented by $h/R = 1.2$, particularly strong negative 'spikes' of C_L occur. They are of consistently large magnitude. Moreover, the positive peaks of C_L are also remarkably consistent, showing three successive peaks for each half-cycle of the cylinder motion.

The C_L variations corresponding to the first cycle of the cylinder motion of figure 2 are shown in expanded form in figure 3, in order to compare the relative magnitudes of the negative peaks as a function of cylinder submergence and, more importantly, to emphasize the phase shift of these peaks relative to one another at different values of h/R. Though the amplitudes of the negative C_L peaks are significantly attenuated

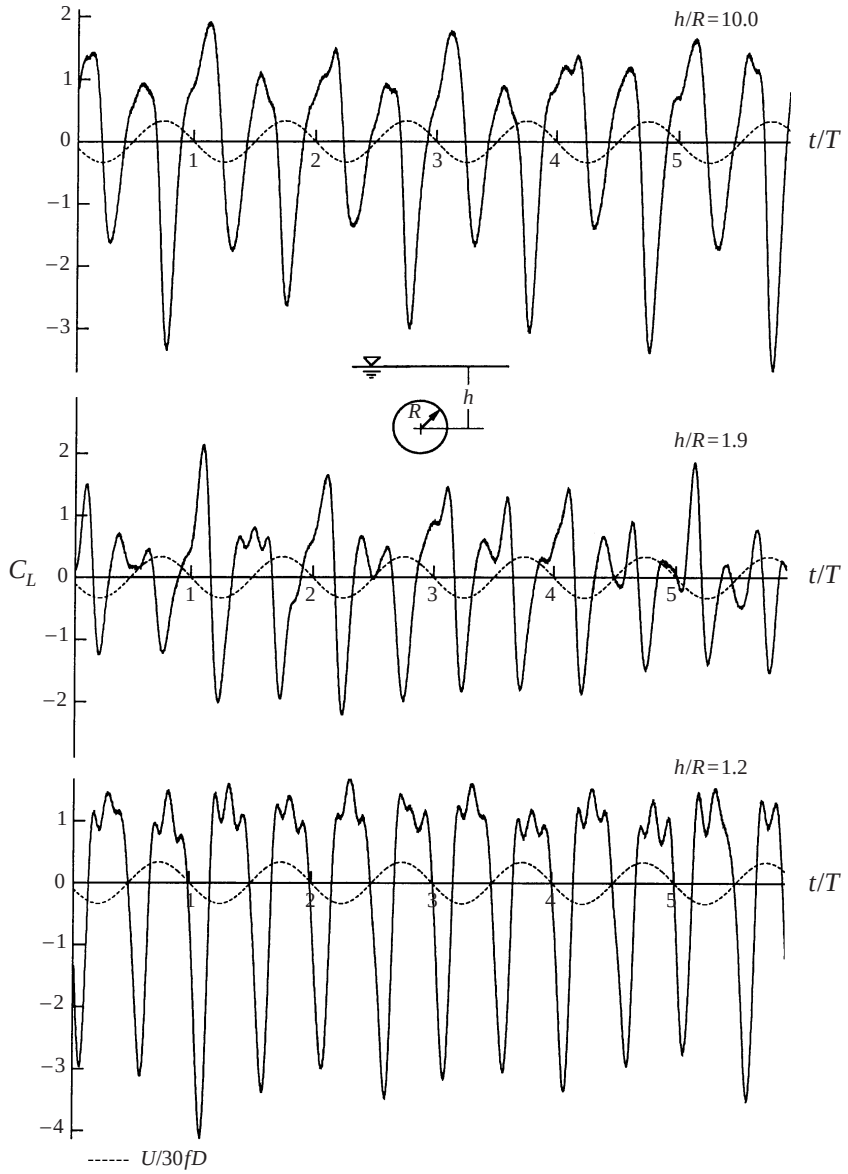

FIGURE 2. Variation of transverse force coefficient C_L as a function of time t normalized by the period T of the cylinder oscillation for three different values of depth of submergence h normalized by the cylinder radius R. – – –, variation of cylinder velocity U normalized by frequency f of oscillation period and cylinder diameter D. Time $t/T = 0$ corresponds to completion of 50th cycle of the cylinder oscillation.

at $h/R = 1.9$ relative to $h/R = 10.0$, they undergo relatively little shift in phase, evident by comparing the vertical dashed lines passing through each trough of the C_L signature. An important, unclarified issue is whether certain features of the patterns of vortex formation and development are maintained at $h/R = 1.9$, relative to those at $h/R = 10$. In contrast, when the cylinder is located immediately beneath the free surface, at $h/R = 1.2$, a dramatic phase shift of the negative spikes of C_L occurs. These spikes are consistently large and advanced in phase relative to cases of deeper

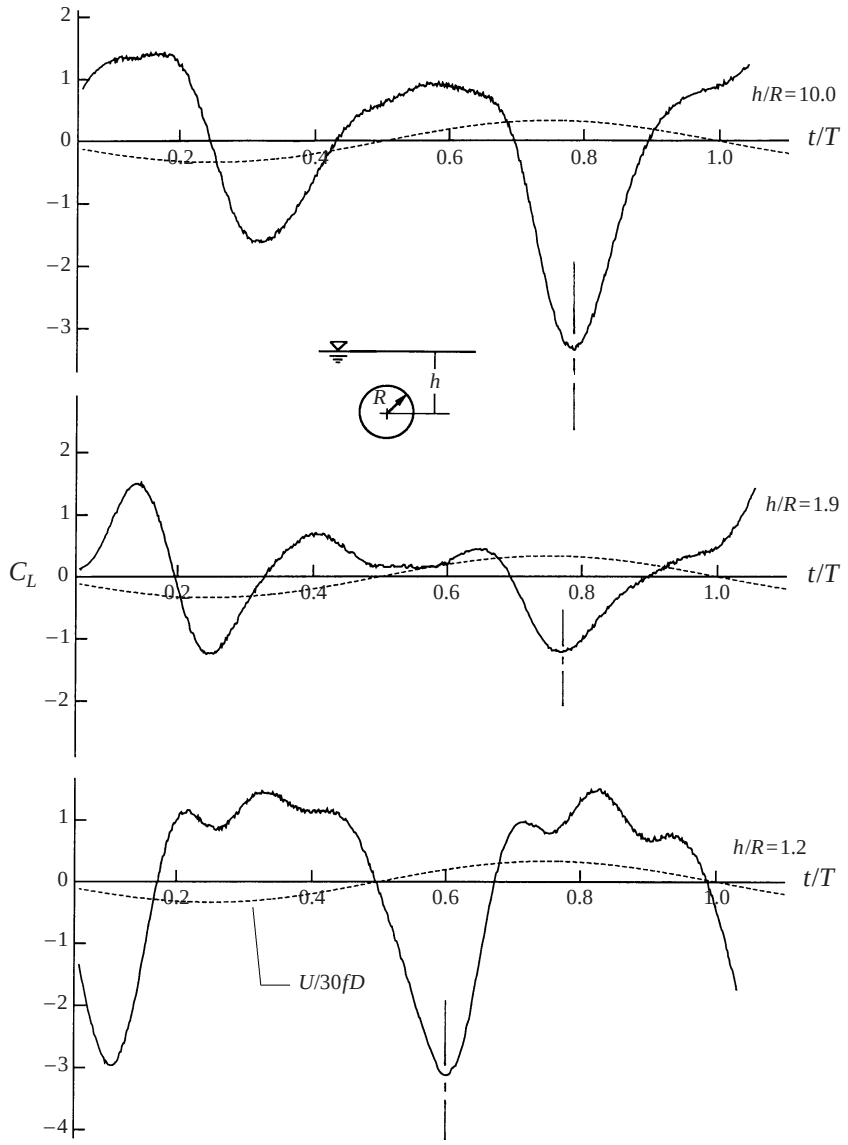

FIGURE 3. Variation of transverse force coefficient C_L over approximately one period of the cylinder oscillation. Time $t/T = 0$ corresponds to completion of 50th cycle of the cylinder oscillation.

submergence, i.e. $h/R = 1.9$ and 10. This observation implies a fundamental change in the corresponding pattern of vortex formation, as yet uninvestigated. In the following, details of the vortex formation process and its consequence for the induced transverse force are addressed.

4. Submerged cylinder: mechanisms of vortex formation and induced transverse force

Patterns of vorticity and velocity are shown in figures 4(*a*) and 4(*b*) as a function of dimensionless time t/T. The corresponding variation of velocity U of the cylinder

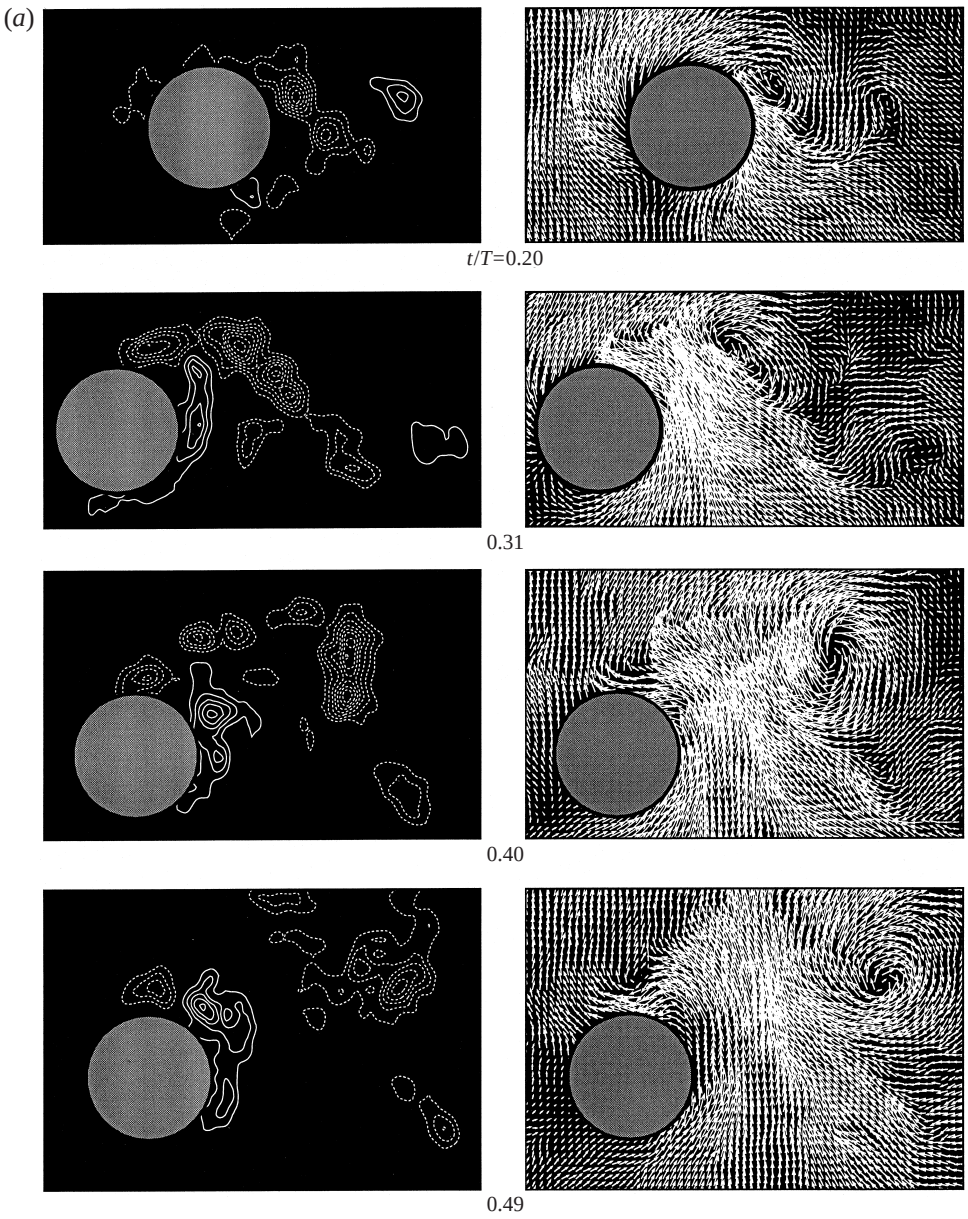

FIGURE 4(*a*). For caption see facing page.

over the oscillation cycle is given in figure 3. For the first part of the oscillation cycle, represented in figure 4(*a*), the cylinder moves to the left with increasing t/T. Development of the layer of negative (dashed line) vorticity from the upper surface of the cylinder, shown at instants $t/T = 0.20$, 0.31, and 0.40, involves small-scale concentrations of vorticity akin to the small-scale vortices observed from a stationary cylinder in steady flow at sufficiently high Reynolds number. They arise from the Kelvin–Helmholtz instability of the separating layer and are known as Bloor–Gerrard vortices, based on the investigations of Bloor (1964) and Gerrard (1978), and characterized subsequently in the studies of Chyu & Rockwell (1996), and Prasad &

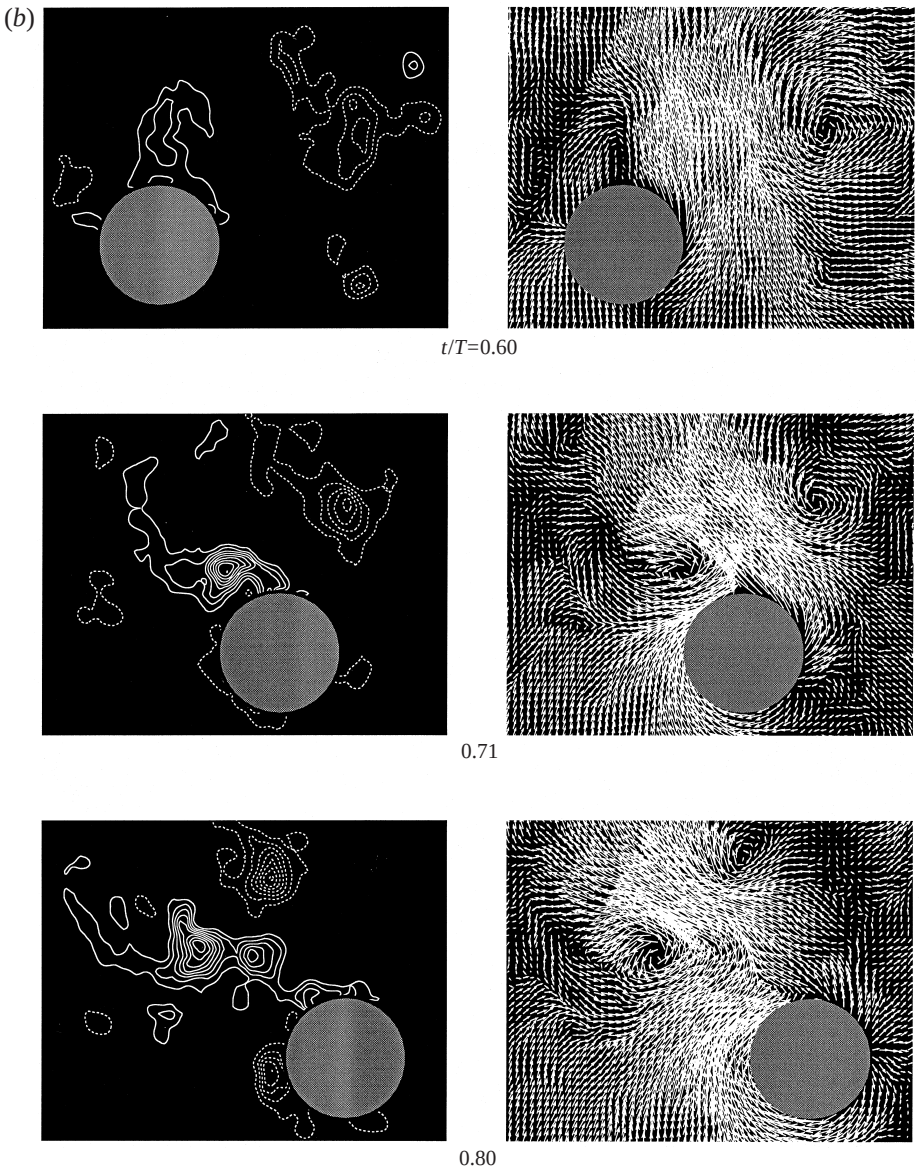

FIGURE 4. Patterns of positive (solid line) and negative (dashed line) vorticity in relation to instantaneous patterns of velocity at key instants during the oscillation cycle. Minimum vorticity level $\omega_{min} = \pm 3\,\mathrm{s}^{-1}$ and incremental vorticity level $\Delta\omega = 3\,\mathrm{s}^{-1}$. $h/R = 10$.

Williamson (1997), and a range of other investigations cited therein. The agglomeration of the small-scale vortices into a larger-scale vortex, evident in comparing images at $t/T = 0.31$ and 0.40, has been addressed recently by Lin & Rockwell (1997), who focused on the comparison of relative values of circulation of the multiple vorticity concentrations and their relation to streamline topology in various reference frames. The circulation $\Gamma^* = \Gamma/\pi U_m D$, in which U_m is the maximum velocity of the cylinder, is -0.83 for the agglomerated, large-scale concentration of negative vorticity at $t/T = 0.40$. The net value of circulation for all remaining small-scale concentrations

is $\Gamma^* = -0.64$. In contrast to the development of this negative layer of vorticity, the positive layer along the surface of the cylinder, first evident at $t/T = 0.31$, does not develop in the same manner as its negative counterpart. Rather, at successive instants $t/T = 0.40$ and 0.49, it exhibits a pronounced concentration of vorticity, which tends to move around the surface of the cylinder, rather than departing from the surface.

The corresponding velocity fields shown in the right-hand column of figure 4(*a*) generally exhibit large-scale swirl patterns of velocity vectors in accord with the major concentrations of vorticity. Other regions of vorticity, however, including that associated with development of a positive vortex along the surface of the cylinder, are not indicated by the velocity patterns. A general feature of the velocity fields of figure 4(*a*) is development of a large-scale, jet-like region between the cylinder and the major swirl pattern. It is oriented in the upward direction and is induced by the major concentration of negative vorticity, evident in the images at $t/T = 0.31$ to 0.49. The width of this jet-like region increases with t/T, corresponding to increased displacement between the major concentration of vorticity and the centre of the cylinder.

The subsequent half of the oscillation cycle, corresponding to rightward movement of the cylinder and positive values of velocity U (cf. figure 3) is represented by the images in figure 4(*b*). At $t/T = 0.60$, the positive region of vorticity along the surface of the cylinder is now oriented vertically above the cylinder and, at subsequent instants of time, unfurls to the left, while the continuously shed vorticity becomes increasingly concentrated into well-defined vortical structures. At times $t/T = 0.71$ and 0.80, the development of this positive vorticity layer is conceptually similar to the negative layer during the first half of the oscillation cycle shown in figure 4(*a*). Simultaneously, a layer of vorticity of opposite (negative) sense concentrates along the lower surface of the cylinder at $t/T = 0.80$; it is the counterpart of the positive concentration formed along the surface shown during the first half of the cycle at $t/T = 0.31$. A distinguishing feature of the patterns of vorticity formed over the second half of the oscillation cycle is the presence of the large-scale, negative concentration of vorticity, evident in the right-hand half of the image at $t/T = 0.60$, which was formed during the earlier part of the cycle. It eventually forms a counter-rotating vortex pair with the large-scale positive concentration of vorticity, as demonstrated at $t/T = 0.80$.

The primary features of the patterns of velocity vectors shown in figures 4(*a*) and 4(*b*) are in general accord with patterns deduced from qualitative dye and particle streak visualization, reviewed by Sarpkaya & Isaacson (1981), Bearman *et al.* (1981), Williamson (1985) and Obasaju *et al.* (1988). The movement of a previously shed vortex past the cylinder and subsequent formation of a vortex pair are evident in these studies. More specifically, the patterns of particle streak visualization of Williamson (1985) provide the equivalent of instantaneous velocity and streamline patterns in the laboratory frame. The velocity field image at $t/T = 0.80$ in figure 4(*b*) is remarkably similar to the particle streak pattern of Williamson (1985, figure 7*a*).

From evolution of the flow patterns shown in figures 4(*a*) and 4(*b*), it is evident that the onset and development of vortex formation from the oscillating cylinder involves a particularly complex series of events, relative to its simpler counterpart of vortex formation from a stationary cylinder in a steady stream. In order to define the mechanisms of vortex formation, it is necessary to compare directly the instantaneous distributions of vorticity and velocity and the streamline topology in the immediate vicinity of the cylinder. After examination of a total of thirty-six sequential images, it was found that the principal features of the vortex development from the cylinder could be described on the basis of five sets of images, selected at crucial instants,

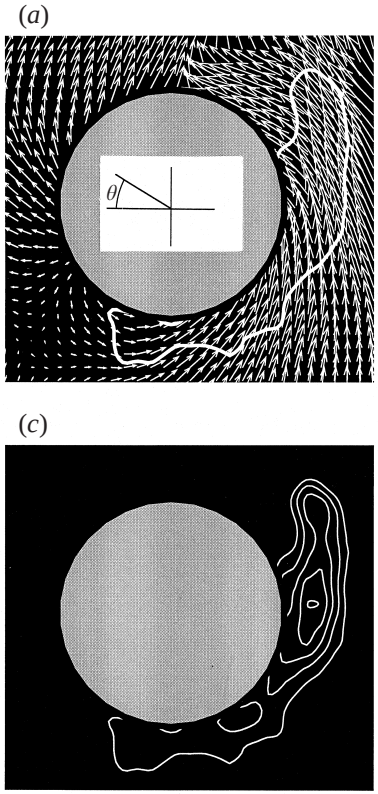

FIG. 5

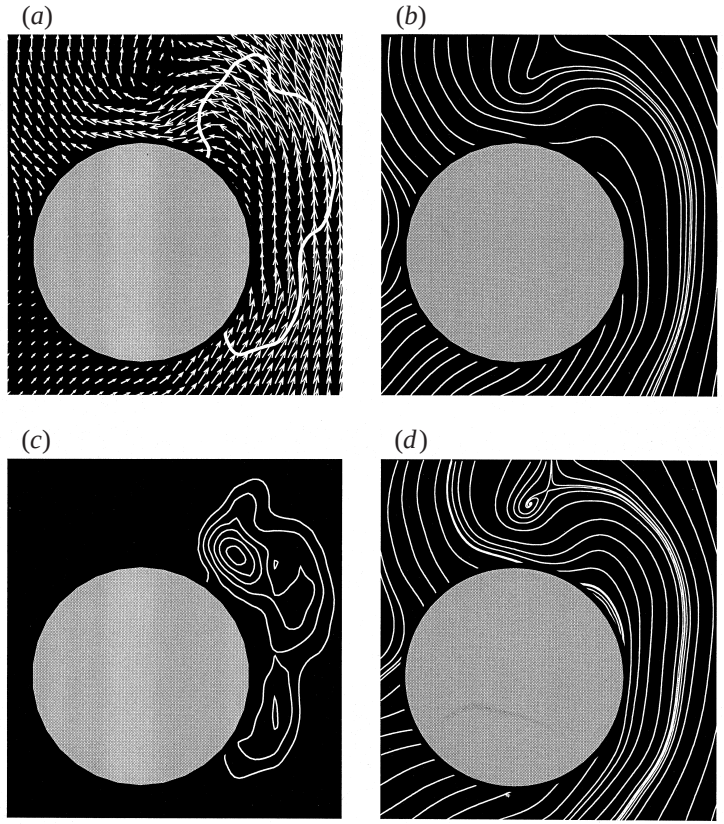

FIG. 6

FIGURE 5. (*a*) Pattern of instantaneous velocity in the laboratory reference frame in relation to a reference contour of positive vorticity (solid white line); (*b*) corresponding pattern of streamline topology in the laboratory frame; (*c*) positive vorticity contours; and (*d*) streamline pattern in the cylinder reference frame. Images correspond to the instant $t/T = 0.31$ during the oscillation cycle of the cylinder. $h/R = 10$.

FIGURE 6. Same as figure 5, except images correspond to the instant $t/T = 0.49$ during the oscillation cycle of the cylinder.

corresponding to figures 5 to 9. These images focus on the development of the positive vorticity adjacent to the surface of the cylinder and its eventual shedding into the cylinder wake. As a consequence, corresponding negative contours of vorticity, exhibited in the overviews of figures 4(*a*) and 4(*b*), are not shown. The five distinct phases of vortex formation initiate with the growth of an attached vorticity layer along the cylinder and conclude with the onset of a classical, separated vorticity layer involving formation of a vortex pattern in the near-wake.

4.1. *Growth of attached vorticity layer*

Figure 5 represents the layer of vorticity along the surface of the cylinder in terms of: (*a*) the instantaneous velocity field in the laboratory frame superposed on the lowest level vorticity contour; (*b*) the streamline pattern in the laboratory frame; (*c*) a complete representation of contours of constant positive vorticity; and (*d*) streamlines in the cylinder reference frame. The angle θ, defined in the inset of figure 5(*a*), is used to aid definition of predominant features of the flow in this and subsequent sets of images. The velocity field and the streamline topology in the laboratory reference frame, illustrated in figures 5(*a*) and 5(*b*), show existence of a saddle point (intersecting streamlines) at $\theta = 315^\circ$ displaced well away from the surface of the cylinder. At the surface of the cylinder, and at approximately the same value of θ, separaticies of a number of streamlines are evident. These streamlines form a bubble along the surface of the cylinder from $\theta = 250^\circ$ to 325°. The lower left-hand boundary of the vorticity contour of figure 5(*a*) lies within this bubble-like region. These observations suggest that the corresponding pressure gradient along the surface of the cylinder in this region is large and serves as a source of vorticity flux. The concentration of vorticity at $\theta = 180^\circ$, illustrated in figure 5(*c*), is apparently the culmination of the vorticity flux through the surface at earlier times. The streamline pattern in a reference frame with respect to the cylinder, shown in figure 5(*d*), suggests half-saddle points at $\theta = 105^\circ$ and 340°. This streamline pattern resembles that of a steady uniform flow at angle-of-attack past a cylinder with bound circulation. It is evident that the extreme reference frames for observing the streamlines, corresponding to figures 5(*b*) and 5(*d*), provide no indication of the vorticity concentration along the surface of the cylinder.

4.2. *Migration of vorticity pattern about circumference of cylinder*

At a later instant, corresponding to $t/T = 0.49$, shown in figure 6, the instantaneous velocity U of the cylinder is nearly zero (cf. figure 3). The pattern of vorticity originally defined in figure 5 has moved circumferentially in the counterclockwise direction about the cylinder. In addition, the extremum of vorticity now has a significantly larger value, indicating further agglomeration into a pronounced vorticity concentration, which is centred at $\theta = 124^\circ$. The velocity field of figure 6(*a*) and the corresponding streamline pattern of figure 6(*b*), both in the laboratory frame, show no indication of significant flow separation from the surface of the cylinder. In the cylinder frame, however, the streamline pattern exhibits a thin separation bubble centred at $\theta = 145^\circ$.

FIGURE 7. Same as figure 5, except images correspond to the instant $t/T = 0.60$ during the oscillation cycle of the cylinder.

FIGURE 8. Same as figure 5, except images correspond to the instant $t/T = 0.69$ during the oscillation cycle of the cylinder.

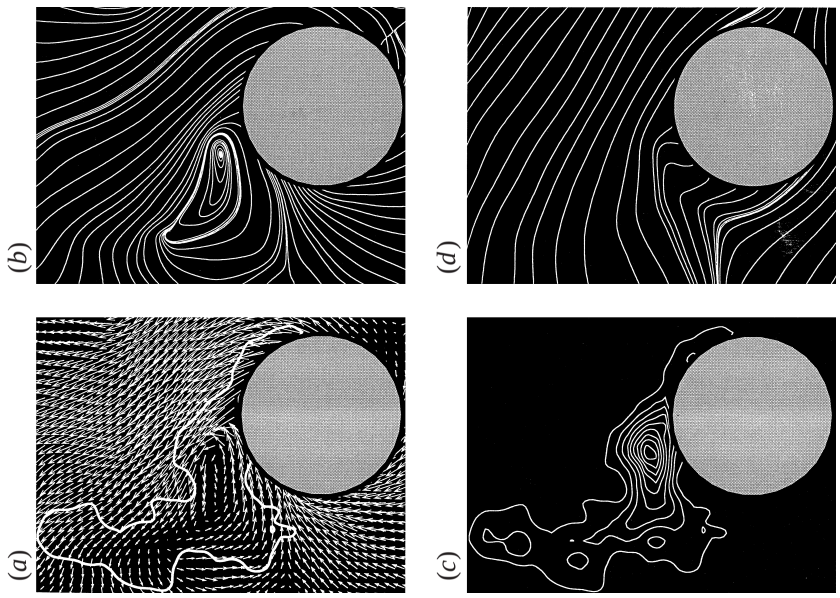

FIG. 8

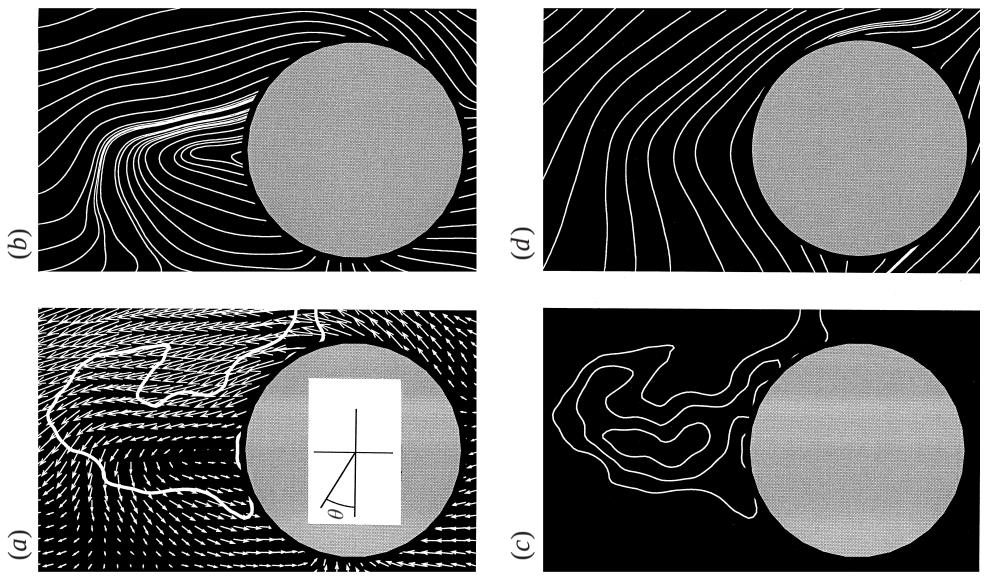

FIG. 7

FIGURES 7 and 8. For captions see facing page.

4.3. *Development of large-scale separation bubble*

Further evolution of the vorticity pattern involves separation from, then reattachment to, the upper surface of the cylinder as indicated in figure 7. The velocity vectors within the vorticity contour of figure 7(*a*) show upward-oriented vectors on the right-hand side, and lower-oriented vectors on the left-hand side, with very low-magnitude vectors between them. The vectors in the vicinity of the cylinder over the range of $\theta = 20^\circ$ to 120° indicate multiple separation and reattachment points, which are further evident in the corresponding streamline pattern of figure 7(*b*). The nested streamlines therein indicate a bubble-like region. A well-defined vorticity concentration is indicated in figure 7(*c*). It is now located well away from the surface of the cylinder; this extremum corresponds to the large velocity gradient occurring between the counter-flowing upward and downward regions of velocity indicated in figure 7(*a*). In the cylinder reference frame of figure 7(*d*), half-saddle points occur at $\theta = 6^\circ$ and 220°. Again, the streamline topologies of figure 7(*b*) and 7(*d*) provide no clear indication of the region of large-scale vorticity.

4.4. *Onset of terminal state of separation bubble*

Continued development of the aforementioned pattern of vorticity involves two basic effects: (i) Unfurling of the pattern of vorticity to the left, as shown in figure 8(*a*), corresponding to movement of the entire pattern in the counterclockwise direction; and (ii) continued flux of vorticity from the surface of the cylinder. Both of these effects give rise to an elongated layer of vorticity. The velocity pattern exhibits a well-defined swirl within the lowest level vorticity contour of figure 8(*a*). The streamline topology in the laboratory reference frame of figure 8(*b*) indicates a pattern of nested streamlines within a limit cycle, in turn within the large-scale separation bubble, which has now moved substantially in the counterclockwise direction from its original position in figure 7(*b*). The extreme separation and reattachment points of this large-scale bubble are bounded by the range from $\theta = 30^\circ$ to 80°. The focus (centre) of the nested streamline pattern in figure 8(*b*) corresponds to the extremum of vorticity indicated in figure 8(*c*). The streamline topology in the cylinder frame of figure 8(*d*) shows no indication of the existence of the vorticity concentration indicated in figures 8(*b*) and 8(*c*).

4.5. *Collapse of large-scale bubble and onset of classical separated vorticity layer*

At the instant corresponding to figure 9, the large-scale bubble indicated in the foregoing images of figures 7 and 8 is not evident. The swirl patterns of the velocity field and the superposed vorticity contour of figure 9(*a*) suggest a separated shear layer of the classical form, involving a sequence of vorticity concentrations. The separation point from the cylinder is sharply defined. It occurs at approximately $\theta = 75^\circ$, at the confluence of the clockwise velocity field about the cylinder for $\theta \lesssim 75^\circ$ and the counterclockwise-oriented velocity field for $\theta \gtrsim 75^\circ$. The topology in the laboratory reference frame of figure 9(*b*) clearly indicates this separation (half-saddle) point. Only the larger-scale vorticity concentration of the actual vorticity field of 9(*c*), however, is represented by this topology. Finally, the streamline topology of figure 9(*d*) suggests a half-saddle at approximately the separation point $\theta \cong 58^\circ$, but only a mild indication of the actual vorticity concentrations present in the flow.

4.6. *Relation of patterns of vorticity to transverse force*

Selected distributions of instantaneous vorticity are shown in figure 10 in relation to the time history of the transverse force coefficient C_L. In this and subsequent

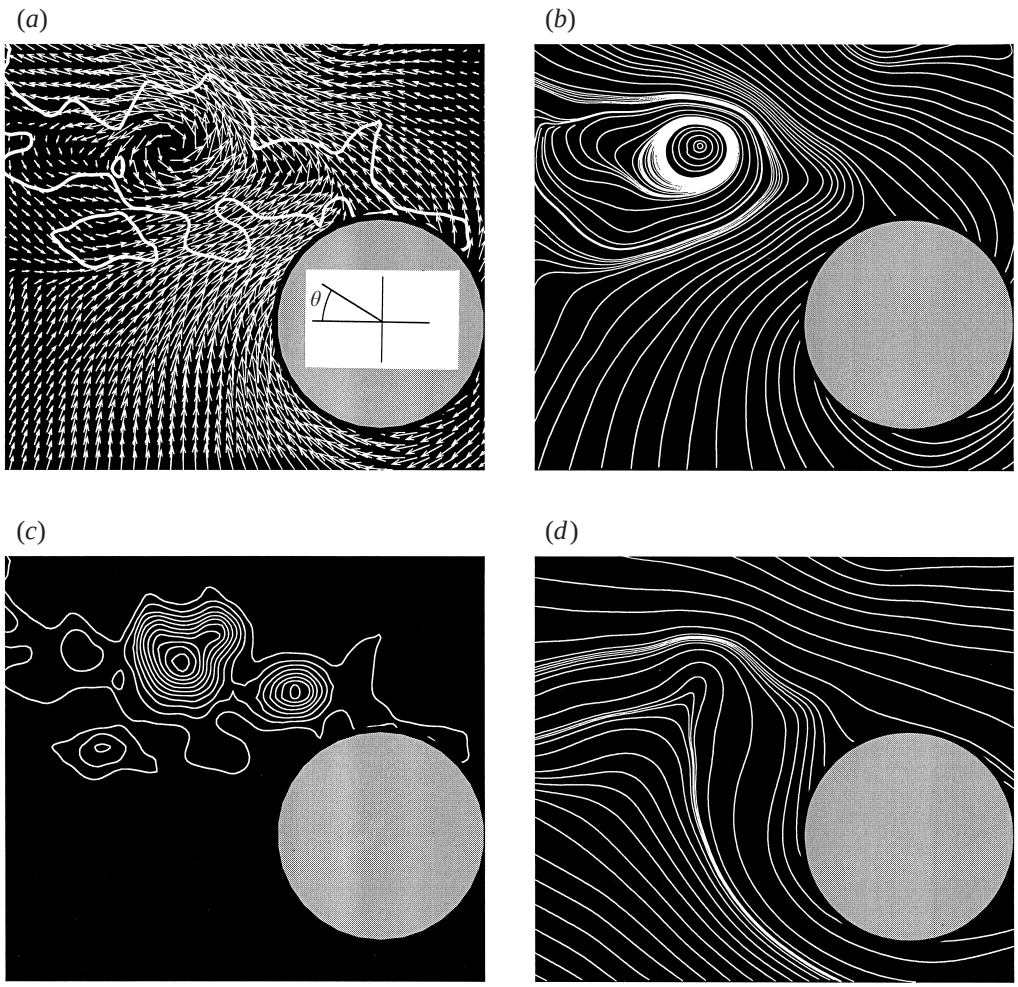

FIGURE 9. Same as figure 5, except images correspond to the instant $t/T = 0.78$ during the oscillating cycle of the cylinder.

sections, emphasis is on the rapidly evolving vorticity concentrations in the vicinity of the cylinder, which are central to determining the instantaneous transverse force. It should be emphasized, however, that all previously shed vorticity must be accounted for in exact calculations of the transverse force. During preliminary diagnostics, which considered regions beyond the field of view employed herein, the circulation of the vorticity concentrations was observed to rapidly decrease, suggesting that the near-wake vorticity exerts a substantial influence on the transverse force. For the first half of the cycle for which the cylinder has a negative velocity U, the magnitude of C_L decreases dramatically from $t/T = 0.20$ to 0.31. Correspondingly, the pattern of negative vorticity moves up and away from the cylinder and abrupt onset of a positive layer of vorticity occurs near its base. For the second half of the cycle, the abrupt drop in C_L, from its maximum-positive value at $t/T = 0.60$ to its maximum-negative value at 0.80, again corresponds to the development of vorticity concentrations in the separated layer, which rapidly moves away from the cylinder. In addition, the large-scale concentration of negative vorticity assumes successive positions such that it eventually forms a counter-rotating vortex system with the

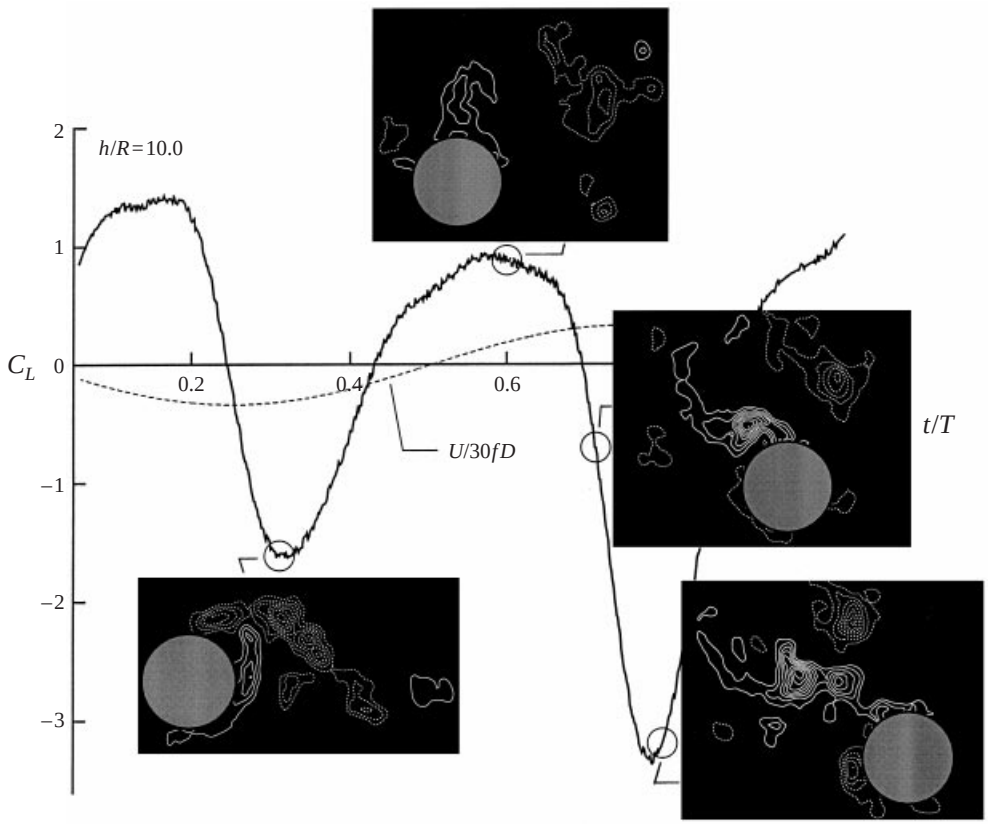

FIGURE 10. Comparison of instantaneous vorticity contours in relation to the variation of the instantaneous transverse force coefficient C_L as a function of dimensionless time t/T. Minimum vorticity level $\omega_{min} = \pm 3\,\mathrm{s}^{-1}$ and incremental vorticity level $\Delta\omega = 3\,\mathrm{s}^{-1}$. $h/R = 10$.

positive vorticity concentrations. In accord with the reasoning of Maull & Milliner (1978), by using point vortices, in conjunction with the Blasius theorem, movement of the vorticity concentrations formed in the separating shear layer, in a direction up and away from the centre of the cylinder, induces negative transverse force and contributes to the negative spikes of C_L at $t/T = 0.3$ and 0.8.

Close to the occurrence of maximum-negative C_L, in the vicinity of $t/T = 0.8$, the concentrations of vorticity are displaced substantially from one instant to the next as indicated in the time sequence of figure 11. The left-hand column shows closely spaced images corresponding to $t/T = 0.77$, 0.80, and 0.83. This outward movement of vorticity, which contributes to the magnitude of the negative transverse force spike, involves agglomeration of the individual (positive) concentrations of vorticity into a single, larger-scale concentration. During this process, the negative vorticity concentration remains intact. Simultaneously, the negative vorticity layer separating from the bottom surface of the cylinder takes on a pronounced form with larger peak levels of vorticity with increasing time. Alternatively, the contribution of the discrete vorticity concentrations to the negative spike of the transverse force, indicated in figure 10, can be assessed by calculating changes with time of moments of vorticity, as undertaken by Lin & Rockwell (1996). If the spatial patterns of vorticity exhibit rapid changes with time, the corresponding vorticity moments will change accordingly. As an indication of the variation of the spatial patterns of vorticity,

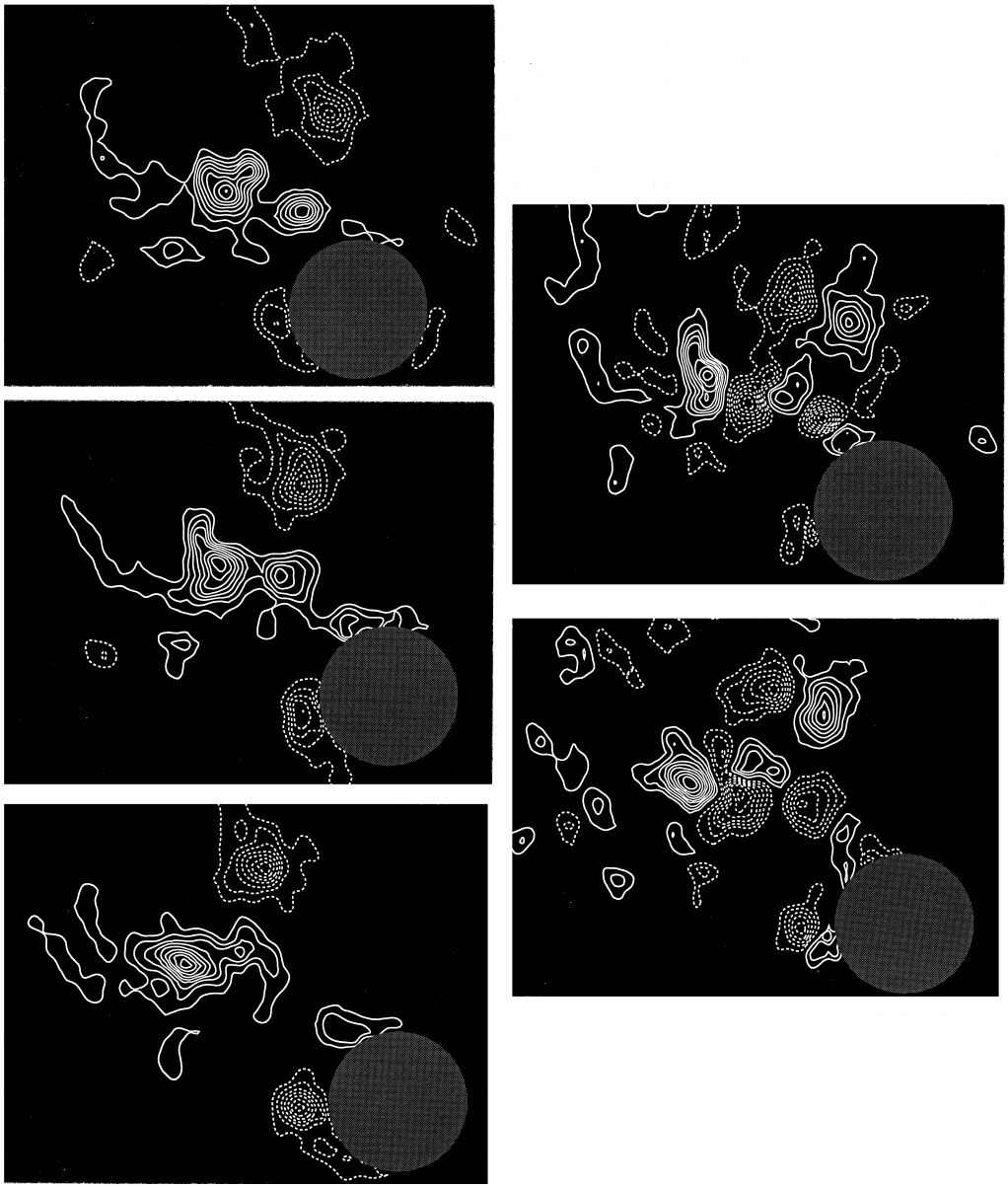

FIGURE 11. Sequence of images closely spaced in time (left-hand column) showing instantaneous contours of positive (solid line) and negative (dashed line) vorticity, approximately corresponding to the occurrence of the negative spike of transverse force. Contours of constant difference vorticity ω_{diff} (right-hand column) are obtained by subtracting vorticity levels in two successive images. Minimum vorticity level $\omega_{min} = \pm 3\,\mathrm{s}^{-1}$ (left- and right-hand columns) and incremental vorticity level $\Delta\omega = 3\,\mathrm{s}^{-1}$ (left-hand column) and $2\,\mathrm{s}^{-1}$ (right-hand column).

differences in vorticity were calculated. In the right-hand column of figure 11, the contours of constant difference vorticity $\Delta\omega$ are illustrated, in order to emphasize the relative displacement of the concentrations of vorticity. These contours are obtained by subtracting the vorticity fields of two successive frames. The image at the upper right-hand side corresponds to the difference between frames at $t/T = 0.80$ and 0.77,

(*a*)

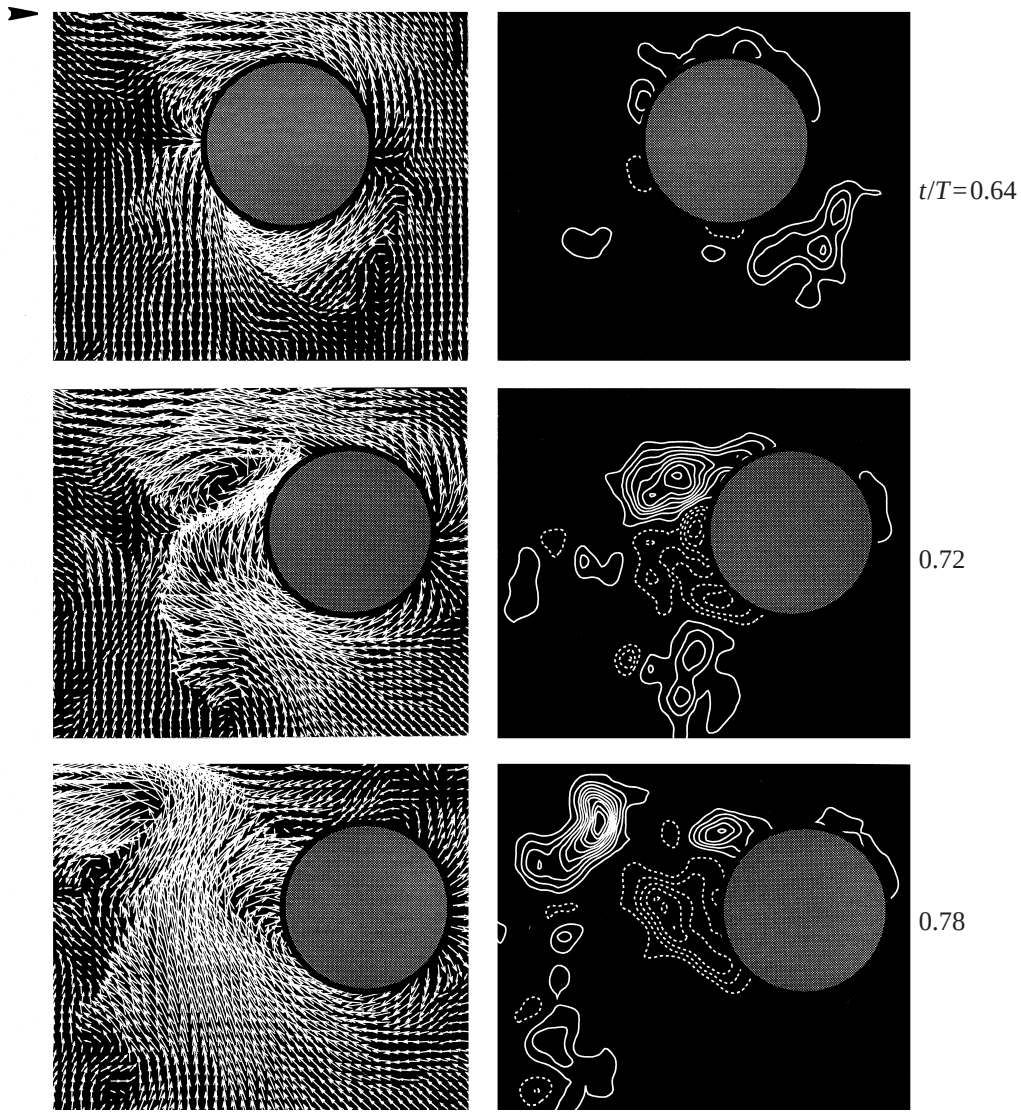

FIGURE 12(*a*). For caption see facing page.

while the bottom right-hand image corresponds to the difference between $t/T = 0.83$ and 0.80. The result is, in general, two rows of alternating concentrations of $\Delta\omega$ that have the highly ordered form depicted in the upper right-hand image. The ordered nature of this pattern is distorted in the image at the lower right-hand side, owing to the agglomeration of the positive concentrations of vorticity mentioned previously.

5. Cylinder in proximity of free surface: vortex patterns and induced transverse force

On the basis of the force traces shown in figure 3, it is evident that proximity of the free surface may alter both the magnitude and phase of transverse force coefficient

(*b*)

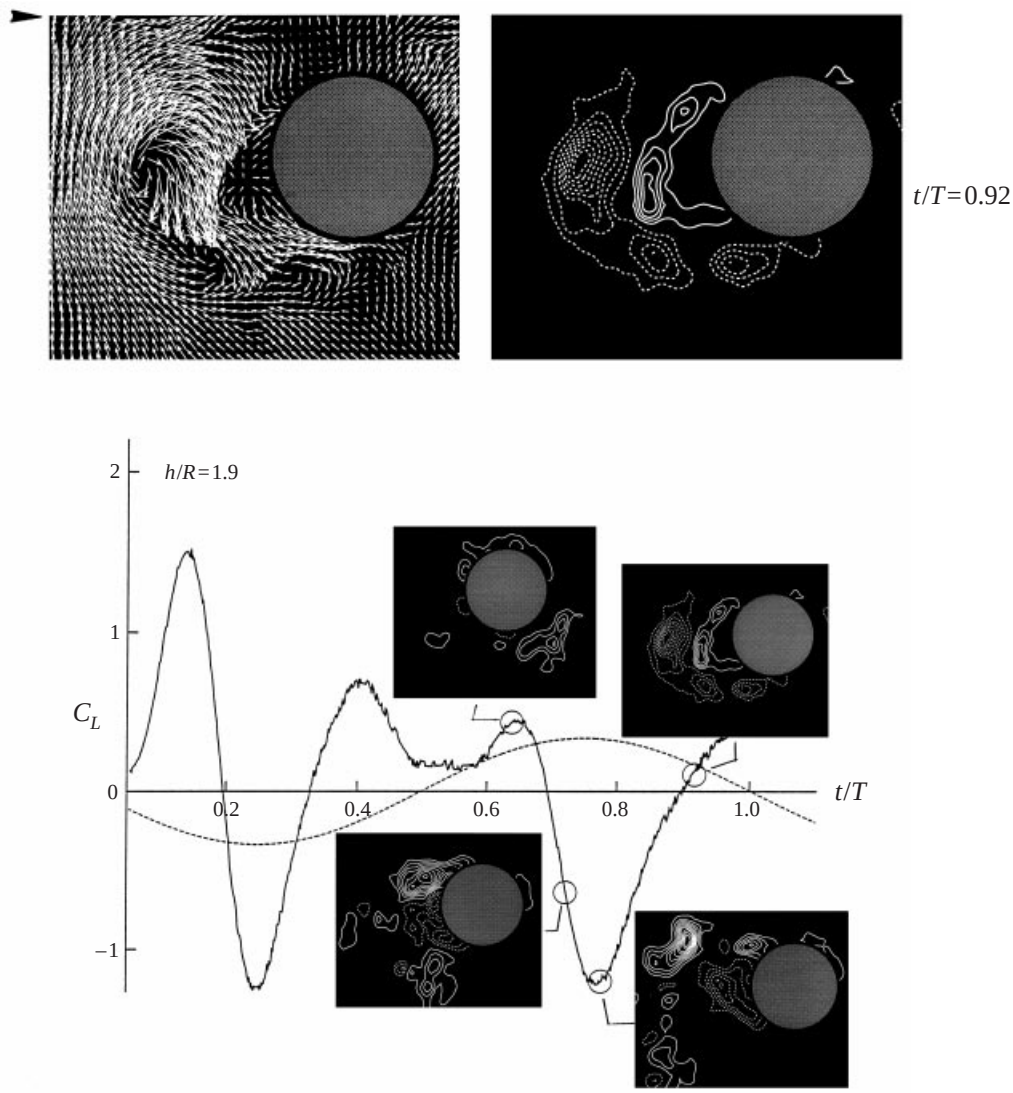

FIGURE 12. (*a*) Patterns of instantaneous positive (solid line) and negative (dashed line) vorticity and instantaneous velocity at the instants $t/T = 0.64$, 0.72 and 0.78 during the oscillation cycle. Minimum vorticity level $\omega_{min} = \pm 3\,\mathrm{s}^{-1}$ and incremental vorticity level $\Delta\omega = 3\,\mathrm{s}^{-1}$. Depth of submergence $h/R = 1.9$. (*b*) At the instant $t/T = 0.92$ during the oscillation cycle. Also shown is the relationship between the instantaneous transverse force signature and representative patterns of vorticity.

C_L, relative to its counterpart for the fully submerged cylinder. In the following, we aim to clarify the underlying physics. For the case where a significant gap exists between the free surface and the upper surface of the cylinder, i.e. $h/R = 1.9$, the transverse force variation of figure 3 shows a substantial reduction in amplitude, but little change in phase of the maximum-negative peaks of C_L relative to the fully submerged counterpart at $h/R = 10$. The velocity and vorticity patterns in the vicinity of the negative peak at $t/T = 0.78$ are given in the bottom row of images

of figure 12(*a*). In this layout, the arrow at the upper left-hand side of the layout of images defines the location of the free surface. The presence of the free surface generally inhibits large-scale transverse motion of the cylinder wake, evident in the velocity fields of the first two images corresponding to $t/T = 0.64$ and 0.72. At later instants, represented by the bottom image of figure 12(a) and the top image of figure 12(*b*), taken at $t/T = 0.78$ and 0.92, large-scale swirl patterns suggest presence of corresponding patterns of vorticity in the wake of the cylinder. These velocity patterns are distinctly different from those of the completely submerged cylinder at the same phase of the cylinder motion, i.e. compare instants $t/T = 0.60$, 0.71, and 0.80 in figure 4(*b*).

The corresponding concentrations of vorticity, shown in the right-hand columns of figures 12(*a*) and 12(*b*) indicate the following sequence. A previously shed positive (grey) concentration of vorticity is swept beneath the surface of the cylinder in the first image ($t/T = 0.64$), and continues its general direction of movement relative to the cylinder in the second image ($t/T = 0.72$); at this instant, however, both positive and negative concentrations of vorticity have been shed from the upper and lower surfaces of the cylinder and, together with the previously shed (positive) concentration beneath them, form a triplet of vertically stacked, alternating concentrations of vorticity. At a later time, shown in the third image ($t/T = 0.78$), each of these concentrations moves further from the cylinder, and an additional, positive concentration is shed from the upper surface. Finally, in the last image, shown at the top of figure 12(*b*) ($t/T = 0.92$), the process of shedding of the positive and negative concentrations from the upper and lower surfaces of the cylinder further progresses.

These concentrations of vorticity are shown on the trace of C_L in figure 12(*b*). The occurrence of the maximum-negative C_L at $t/T = 0.78$ has general features in common with its fully submerged counterparts at $t/T = 0.31$ and 0.80 in figure 12(*b*). In both cases, concentrations of vorticity are shed from the top surface of the cylinder, and their movement up/away from the surface of the cylinder contributes to the peak negative C_L. The physics of vortex formation and development from the cylinder adjacent to a free surface is, however, distinguished from that of a fully submerged cylinder in the following respects: (i) a positive concentration of previously shed vorticity is swept beneath the cylinder ($t/T = 0.72$ in figure 12*a*) rather than above the cylinder ($t/T = 0.80$ in figure 4(*b*)); (ii) the positive layer of vorticity remains at approximately the same vertical elevation as the upper surface of the cylinder ($t/T = 0.78$ in figure 12*a*) rather than moving upward from the cylinder ($t/T = 0.80$) in figure 4(*b*); and (iii) formation of the negative concentration of vorticity is more advanced ($t/T = 0.78$) in figure 12(*a*), relative to the initially developed concentration of negative vorticity ($t/T = 0.80$) in figure 4(*b*).

6. Cylinder adjacent to free surface: vortex patterns and induced transverse force

For the case where the cylinder is immediately beneath the free surface, $h/R = 1.2$, the trace of C_L given in figure 3 shows, in comparison with the cases of the more deeply submerged cylinder, a radical shift in timing, i.e. phase, of the negative transverse force spike relative to the cylinder motion. Moreover, these negative spikes of C_L are consistent and pronounced, relative to the aforementioned cases. The corresponding velocity and vorticity patterns are given in figures 13(*a*) and 13(*b*). All images show a significant depression of the free surface immediately above the surface of the cylinder. This depression precludes a jet-like flow through the gap between the cylinder and

the free surface, as was observed in figure 12(*a*). Consider first the images of velocity vectors shown in the left-hand column. In the uppermost image, corresponding to $t/T = 0.34$, a large-scale swirl pattern suggests a corresponding concentration of vorticity at that location. In subsequent images at $t/T = 0.49$ and 0.60, a pronounced jet flow is induced along the lower surface of the cylinder and, at $t/T = 0.71$, a large, clockwise swirl of velocity vectors suggests a vortex immediately behind the cylinder; beneath this swirl, a milder swirl of opposite sense suggests the existence of a positively oriented vortex. These patterns of velocity have no apparent resemblance to their counterparts in figure 12(*a*) e.g. compare patterns at the instant corresponding to maximum-negative transverse force: $t/T = 0.78$ in figure 12(*a*) and $t/T = 0.60$ in figure 13(*a*). It is therefore evident that the presence of the gap has a dominant influence on the entire flow pattern about the cylinder.

Corresponding concentrations of vorticity are given in the right-hand columns of figures 13(*a*) and 13(*b*). At $t/T = 0.34$, the vorticity field is dominated by a positive layer of vorticity shed from the bottom layer of the cylinder, which eventually agglomerates to form a relatively large-scale vortical structure at $t/T = 0.49$. At $t/T = 0.60$, this cluster of vorticity, which has a value of circulation $\Gamma^* = \Gamma/\pi U_m D = 0.92$, moves beneath the cylinder, and at $t/T = 0.71$ coexists with a large-scale negative cluster formed from the lower surface of the cylinder. Vorticity shed from the upper surface of the cylinder has a relatively small spatial extent. Finally, at $t/T = 0.83$, the large-scale cluster of positive vorticity has rapidly moved to the left-hand side out of the field of view, and the negative layer of vorticity continues to shed into the near-wake. This pattern has a form that is nearly the mirror image of the pattern at $t/T = 0.34$.

The instantaneous concentrations of vorticity are shown in conjunction with the time history of C_L in figure 13(*b*). The peak positive values of C_L at $t/T = 0.34$ and 0.83 are in accord with the movement of the large-scale clusters of positive ($t/T = 0.34$) and negative ($t/T = 0.83$) vorticity away from the surface of the cylinder. On the other hand, the peak negative spike of C_L at $t/T = 0.6$ is associated with movement of a large-scale cluster of vorticity beneath the surface of the cylinder. Both of these trends are deducible from the point vortex simulation of Maull & Milliner (1978). We again emphasize that all previously shed vorticity must be accounted for when exactly determining the forces on the cylinder.

In summary, for this case of the cylinder immediately adjacent to the free surface, we have the observation that even though large-scale concentrations of vorticity are shed from only the bottom of the cylinder, the consistency (compare $h/R = 10$ in figure 3) and magnitude (compare $h/R = 1.9$ in figure 3) of the induced transverse force surpass those corresponding to a cylinder at deeper submergence.

7. Concluding remarks

The degree of submergence of the cylinder has a dramatic effect on the type of vortex formation in the near-wake of a cylinder oscillating in quiescent fluid. The principal features of vortex formation have been defined using quantitative representations of the instantaneous flow patterns, i.e. velocity distributions, streamline topology in the laboratory and cylinder reference frames, and vorticity distributions.

For the case of the fully submerged cylinder, the process of vortex formation involves a sequence of complex events, relative to simpler case of Kármán vortex formation in a steady flow. Development and migration of a distributed vorticity layer about the circumference of the cylinder, which may exhibit a localized concentration of vorticity, eventually gives way to shedding of a layer of small-scale

(*a*)

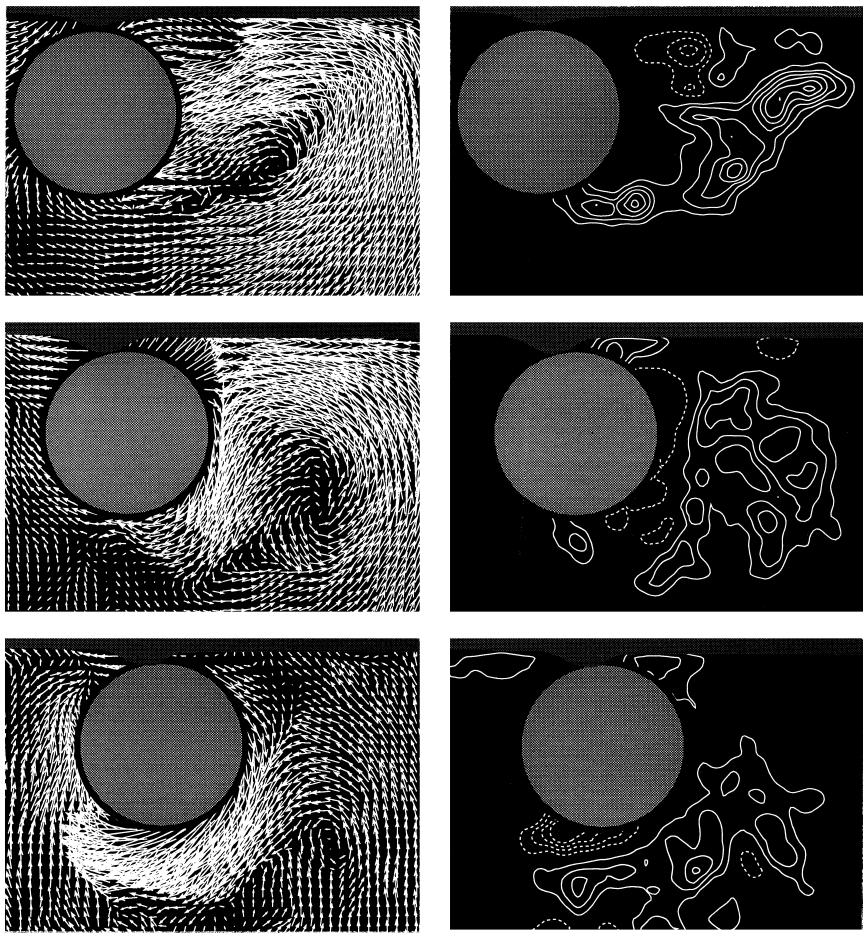

FIGURE 13(*a*). For caption see facing page.

vorticity concentrations, some of which agglomerate to form a large-scale vortex. The corresponding streamline topology allows definition of saddle points, half-saddle points, separatixes and reattachment points during the vortex formation process. Most importantly, vortex development involves formation of a large-scale separation bubble on the surface of the cylinder that eventually collapses at the initiation of classical vortex shedding from the surface of the cylinder. The transverse force signature exhibits highly ordered modulations, which can be related to defined patterns of instantaneous vorticity concentrations. The dominant negative spike of transverse force occurs in conjunction with formation of a counter-rotating vortex pair involving a vorticity concentration shed from the previous cycle.

When the cylinder is adjacent to the free-surface, such that a gap exists between them, the verticle movement of the vorticity layer shed from the cylinder is inhibited. Furthermore, the negative concentration of vorticity formed from the previous cycle is not swept above the cylinder, as in the fully submerged case; rather, the positive concentration shed during the previous cycle is swept beneath the cylinder and forms a vertically stacked system of three vortices in the near-wake. Correspondingly, the amplitude of the negative spikes of C_L is attenuated. The phase of these negative

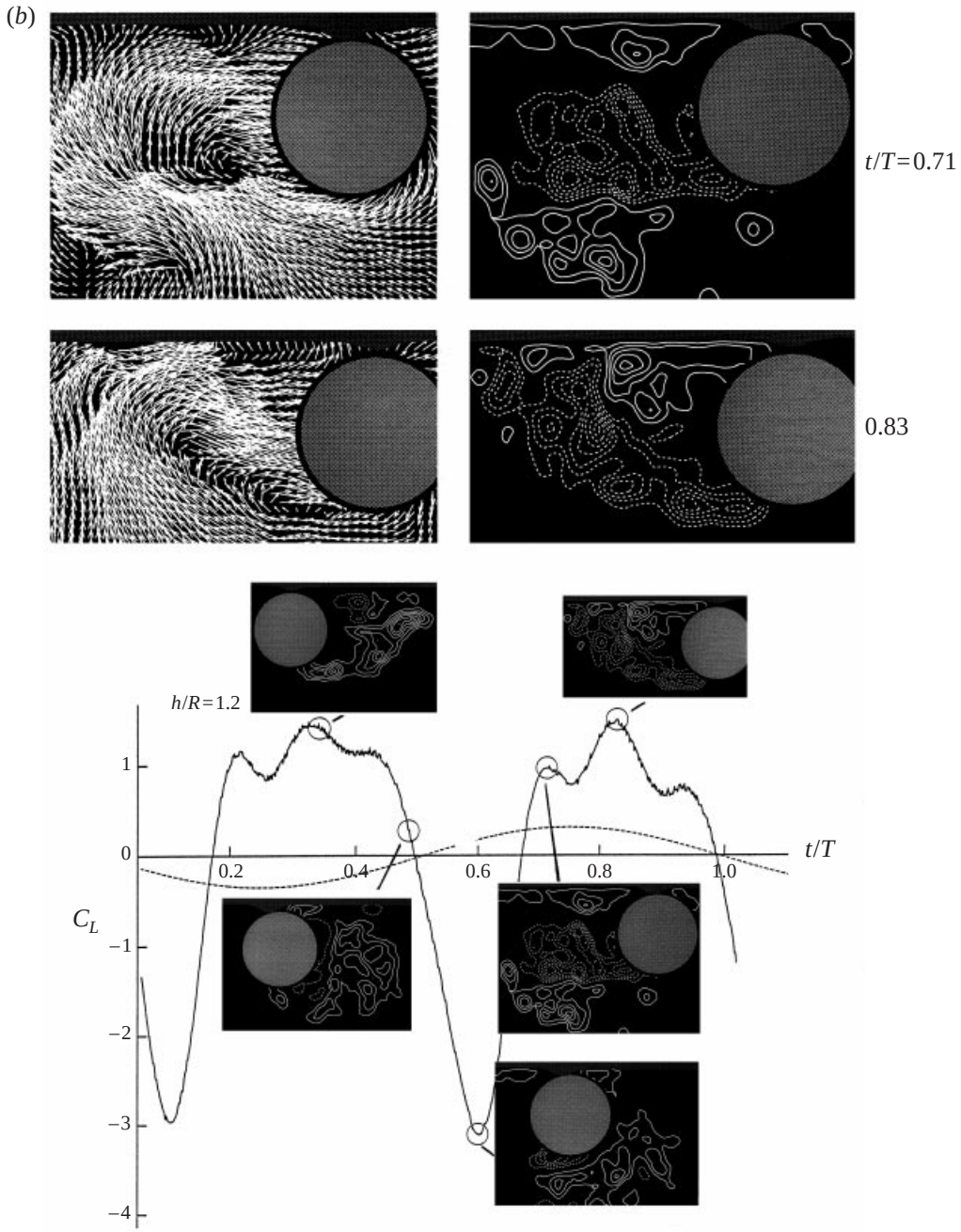

FIGURE 13. (*a*) Patterns of instantaneous positive (solid line) and negative (dashed line) vorticity and instantaneous velocity at the instants $t/T = 0.34$, 0.49, 0.60 during the oscillation cycle. Minimum vorticity level $\omega_{min} = \pm 3\,\mathrm{s}^{-1}$ and incremental vorticity level $\Delta\omega = 3\,\mathrm{s}^{-1}$. Depth of submergence $h/R = 1.2$. (*b*) At the instants $t/T = 0.71$ and 0.83 during the oscillation cycle. Also shown is the relationship between the instantaneous transverse force signature and representative patterns of vorticity.

spikes relative to the cylinder velocity is, however, altered only slightly compared to the fully-submerged cylinder.

For the extreme case where the cylinder is located immediately beneath the free surface, such that no gap region exists, significant vorticity concentrations are formed only from the bottom surface of the cylinder. Remarkably, the negative spikes of transverse force are generally of larger magnitude and more consistent than those for which the cylinder is more deeply submerged. In fact, the vortex–cylinder interaction associated with the negative spikes is fundamentally different. It is dominated by sweeping of a large-scale, positive concentration of vorticity beneath the surface of the cylinder. This positive concentration is formed from the cylinder during a previous cycle; despite the proximity of the cylinder, no pronounced concentrations from the free surface were observed. As a consequence, the transverse force spikes are dramatically shifted in phase, i.e. occur at a different value of the cylinder velocity, relative to the cases of deeper submergence.

Taking an overview of the vortex patterns in the present investigation, it is evident that they are considerably more complex than for Kármán vortex formation from a stationary cylinder in steady flow. This point is abundantly clear from the qualitative flow-visualization studies of a fully submerged cylinder summarized in § 1. For the present case of the fully submerged cylinder, it is evident that the formation of vorticity concentrations in the separated layer is analogous to that in the layer leading to Kármán vortex formation. It occurs, however, only from one (i.e. top) side of the cylinder. Despite the effects of proximity of the free surface on altering the magnitude and phase of the vortex formation process, the alternating formation of positive and negative layers of vorticity from only one side of the cylinder appears to persist for varying degrees of submergence and, in the limiting case of the cylinder immediately adjacent to the free surface, it switches from the top to the bottom surface of the cylinder. Of course, other types of vortex formation simultaneously occur, and the timing of the entire previously shed vortex system is influenced by the proximity of the free surface, in turn altering the magnitude and phase of the transverse force.

Unlike the case of Kármán vortex formation from an oscillating cylinder in a steady stream, it is well known that vortex formation from an oscillating cylinder in a quiescent fluid exhibits more than one admissible mode, at least for the fully submerged cylinder. In fact, Obsaju *et al.* (1988) address this variability of modes for a given set of oscillation parameters. At, for example, $KC = 10$, the general pattern of vortex formation was the same, but could occur at four different angles θ, where θ is the angle measured between the instantaneous, positive flow direction and the path of the vortex pair. In essence, our experiments exhibited a similar variability of occurrence of these four possible modes. A given mode was observed to remain locked-on for a number of cycles before transforming to a different mode. When the cylinder is moved closer to the free surface, the mode of vortex formation does not appear to be an extension of the possible modes that can occur for the essentially, fully submerged cylinder. Rather, new types of modes develop; such modes appear to have one form, i.e. the overall pattern of vortex formation remains generally similar from one cycle to the next. This observation raises the issue of stabilization of an otherwise non-repeatable, or even chaotic, system of vortices due to the proximity of a free surface. This topic deserves theoretical consideration.

The authors are grateful to the Office of Naval Research for support under Grant no. N00014-94-1-0815, P00001, monitored by Dr Thomas Swean. Supplemental

support was provided by NSF Grant No. CTS-9803734, monitored by Drs Roger Arndt and John Foss.

REFERENCES

Anagnostopoulos, P., Iliadis G. & Ganoulis, J. 1995 Flow and response parameters of a circular cylinder vibrating in-line with the oscillating stream. In *Flow-Induced Vibration* (ed. P. Bearman). Balkema, Rotterdam.

Baba, N. & Miyata, H. 1987 Higher-order accurate solutions of vortex generation from a circular cylinder in a oscillatory flow. *J. Comput. Phys.* **69**, 362–396.

Bearman, P. W., Graham, J. M. R., Naylor, P. & Obasaju, E. D. 1981 The role of vortices in oscillatory flow about bluff cylinders. *Intl Symp. on Hydrodyn. and Ocean Engng, the Norwegian Institute of Technology*, pp. 621–644.

Bloor, M. S. 1964 The transition to turbulence in the wake of a circular cylinder. *J. Fluid Mech.* **19**, 290–304.

Chyu, C.-K & Rockwell, D. 1996 Near-wake structure of an oscillating cylinder: effective control of shear-layer vortices. *J. Fluid Mech.* **322**, 21–49.

Gerrard, J. H. 1978 The wakes of cylindrical bluff body at low Reynolds number. *Phil. Trans. R. Soc. Lond.* A **288**, 351–382.

Honji, H. 1981 Streaked flow around an oscillating circular cylinder. *J. Fluid Mech.* **107**, 509–520.

Ikeda, S. & Yamamoto, Y. 1981 Transverse force forces on cylinders in oscillatory flows. *Rep. Dept Foundation of Engineering and Coastal Engineering, Saitama University, Japan*, vol. 10, pp. 1–16.

Iwagaki, Y., Asano, T. & Nagai, F. 1983 Hydrodynamic forces on a circular cylinder placed in wave-current co-existing fields. *Mem. Fac. Engng Kyoto University, Japan*, vol. 45, pp. 11–23.

Jacobsen, V., Bryndum, M. B., Nielsen, R. & Fines, S. 1984 Cross-flow vibrations of a pipe close to a rigid boundary. *Trans. ASME J. Energy Resources Technol.* **106**, 451–457.

Jarno-Dreuaux, A., Sakout, A. & Lambert, E. 1995 Interference between a circular cylinder in a plane wall under waves. *J. Fluids Struct.* **9**, 215–230.

Justesen, P. 1991 A numerical study of oscillating flow around a circular cylinder. *J. Fluid Mech.* **222**, 157–196.

Lighthill, J. 1986 Fundamentals concerning wave loading on off-shore structures. *J. Fluid Mech.* **173**, 667–681.

Lin, J.-C. & Rockwell, D. 1996 Force identification by vorticity fields: techniques based on flow imaging. *J. Fluids Struct.* **10**, 663–668.

Lin, J.-C. & Rockwell, D. 1997 Quantitative interpretation of vortices from a cylinder oscillating in quiescent fluid. *Exps. Fluids* **23**, 99–104.

Lin, J.-C., Sheridan, J. & Rockwell, D. 1996 Near-wake of a perturbed, horizontal cylinder at a free-surface. *Phys. Fluids* **8**, 2107–2116.

Lin, X. W., Bearman, P. W. & Graham, J. M. R. 1996 A numerical study of oscillatory flow about a circular cylinder for low values of beta parameter. *J. Fluids Struct.* **10**, 501–526.

Maull, D. J. & Milliner, M. C. 1978 Sinusoidal flow past a circular cylinder. *Coastal Engng* **2**, 149–168.

Miyata, H. & Lee, Y.-G. 1990 Vortex motions about a horizontal cylinder and waves. *Ocean Engng* **17**, 279–305.

Miyata, H., Shikazono, N. & Kanai, M. 1990 Forces on a circular cylinder advancing steadily beneath the free-surface. *Ocean Engng* **17**, 81–104.

Noca, F. 1997 On the evaluation of time-dependent fluid-dynamic forces on bluff bodies. PhD dissertation, California Institute of Technology.

Noca, F., Shiels, D. & Jeon, D. 1997 Measuring instantaneous fluid dynamic forces on bodies, using only velocity field and their derivatives. *J. Fluids Struct.* **11**, 345–350.

Obasaju, E. D., Bearman, P. W. & Graham, J. M. R. 1988 A study of forces, circulation, vortex patterns around a circular cylinder and oscillating flow. *J. Fluid Mech.* **196**, 467–494.

Prasad, A. & Williamson, C. H. K. 1997 The instability of the shear layer separating from a bluff body. *J. Fluid Mech.* **333**, 375–402.

Rockwell, D., Magness, C., Towfighi, J., Akin, O. & Corcoran, T. 1993 High-image-density particle imagevelocimetry using laser scanning techniques. *Exps. Fluids* **14**, 181–192.

Sarpkaya, T. 1963 Transverse force, drag, and added-mass coefficients for a circular cylinder immersed in a time-dependent flow. *Trans. ASME* E: *J. Appl. Mech.* **85**, 13–15.

Sarpkaya, T. 1968 An analytical study of separated flow about circular cylinders. *Trans. ASME* D: *J. Basic Engng* **90**, 511–520.

Sarpkaya, T. 1969 Analytical study of separated flow about circular cylinders. *Phys. Fluids* **12**, Suppl. II, 145.

Sarpkaya, T. 1986 Force on a circular cylinder in viscous oscillatory flow at low Keulegan–Carpenter numbers. *J. Fluid Mech.* **165**, 61–71.

Sarpkaya, T. 1989 Computation methods with vortices–The 1988 Freeman Scholar Lecture. *Trans. ASME* I: *J. Fluids Engng* **111**, 5–52.

Sarpkaya, T. & Isaacson, M. 1981 *Mechanics of Wave Forces on Offshore Structures*. Van Nostrand Reinhold.

Sheridan, J., Lin, J.-C. & Rockwell, D. 1997 Flow past a cylinder close to a free surface. *J. Fluid Mech.* **330**, 1–30.

Singh, S. 1979 Forces on bodies in oscillatory flow. PhD thesis, University of London.

Sumer, B. M. & Fredsøe, J. 1986 Transverse vibrations of an elastically-mounted cylinder exposed to an oscillating flow. *Proc. Sixth ASME Intl Offshore Mech. and Arctic Engng Symp. Houston, TX*, vol. 2, pp. 165–173.

Sumer, B. M., Fredsøe, J. & Jacobsen, V. 1986 Transverse vibrations of a pipeline exposed to waves. *Proc. Fifth Intl Offshore Mech. and Arctic Engng Symp. Tokyo, Japan*, 13–17 April, vol. 3, pp. 588.

Sun, X. & Dalton, C. 1996 Application of the LES method to the oscillating flow past a circular cylinder. *J. Fluids Struct.* **10**, 851–872.

Szepessy, S. & Bearman, P. W. 1993 Analysis of a pressure averaging device for measuring aerodynamic forces on a circular cylinder. *Exps. Fluids* **16**, 120–128.

Tatsuno, M. & Bearman, P. W. 1990 A visual study of the flow around an oscillating cylinder at low Keulegan–Carpenter numbers and Stokes numbers. *J. Fluid Mech.* **211**, 157–182.

Tsahalis, D. T. 1984 Vortex-induced vibrations of a flexible cylinder near a plane boundary exposed to steady and wave-induced currents. *Trans. ASME J. Energy Resources Technol.* **106**, 206–213.

Tsahalis, D. T. 1985 Vortex-induced vibrations due to steady and wave-induced currents of a flexible cylinder near a plane boundary. *Proc. Fourth Intl Offshore Mech. Arctic Engng Symp. Dallas, TX*, 17–21 February, vol. 1, pp. 618–628.

Unal, M. F., Lin, J.-C. & Rockwell, D. 1997 Force prediction by PIV imaging: a momentum-based approach. *J. Fluids Struct.* **11**, 965–971.

Wang, X. & Dalton, C. 1991 Oscillating flow past a rigid circular cylinder: a finite-difference calculation. *Trans. ASME* I: *J. Fluids Engng* **113**, 377–383.

Williamson, C. H. K. 1985 Sinusoidal flow relative to circular cylinder. *J. Fluid Mech.* **155**, 141–174.